Next Generation Adaptive Optics

DAVINCI Pixel Scales and Sensitivities (KAON 763)

By Sean Adkins and Al Conrad,
with contributions from Mike Fitzgerald and Jim Lyke

December 9, 2009 Revised May 12, 2010 and May 29, 2010

INTRODUCTION

This document describes the proposed pixel scale for the DAVINCI imager and gives a rationale for the selected scales. Because the sensitivity of the instrument is also related to the choice of pixel scale (all other things being equal), an analysis of the expected point source sensitivities over the wavelength range of 0.7 to 2.4 μm is presented. A discussion of representative sensitivities for the DAVINCI IFS is also presented. A future update to this document will include discussion of the sensitivities for extended objects.

The discussion in this document is based on the current DAVINCI optical design (Adkins, et al., 2010) and the DAVINCI background and zero point estimates presented in Adkins and McGrath (2010).

IMAGER PIXEL SCALES

As described in Kupke (2009) the NGAO science relay will offer an unvignetted field of view (FOV) covering 40" diameter. We assume that the NGAO relay offers diffraction limited performance over the full NGAO wavelength range. We also assume that while the Strehl provided by adaptive optics correction will diminish at the shorter wavelengths, the core of the PSF is still equal to the diffraction limited image size even for a comparatively low Strehl.

The discussion of what detector pixel scale or scales should be provided is based on the following considerations:

1. **Spatial sampling**: the imager should provide at least 2 pixel sampling across the FWHM of the Airy disk (~λ/D).
2. **Optimal sampling**: the optimal sampling will require consideration of the signal to noise ratio (SNR) and how the image will be used. In general, when SNR is high, more than two pixel sampling is beneficial, especially for PSF determination, astrometry, and photometry.
3. **FOV**: the FOVs required by the key science drivers range from 4" to 10", with larger FOVs of 15" or more desired for certain science drivers (see Adkins et al., 2009). The minimum FOV should be one that meets as many of the science requirements as possible without becoming a driver on instrument cost (cost will mainly be driven by the size of the clear apertures for the lenses or mirrors in the optical system and the required detector size). The FOV should also be chosen to take full advantage of the field available from the AO system, keeping in mind the fact that Strehl will fall somewhat as the field radius is increased. The FOV should not exceed the FOV of the science relay by any significant amount or expensive detector pixels will go unused.
4. **Background**: the sky background levels in the near-IR, combined with thermal emission from the telescope and AO system, especially in the K-band, result in pixels with larger on sky area (a coarser pixel scale) becoming background limited more quickly than pixels with a smaller on sky area.

5. **Read noise and dark current**: smaller pixels will increase the read noise and dark current noise contribution for a given extended object size.
6. **Imager performance, complexity, and cost**: for reasons of complexity, optical performance, and cost it is desirable to have only one imager spatial sampling scale.
7. **Detector size and pixel dimensions**: the NGAO imager will use a 4096 x 4096 pixel IR focal plane array with 15 μm pixels (the Hawaii-4RG).

With a square detector, the square area that will fall entirely within a 40" diameter FOV is 28.28" x 28.28". Given a 4096 x 4096 pixel detector, the corresponding pixel scale is 7 mas, resulting in a FOV of 28.7" x 28.7". A second candidate is an 8 mas scale, which provides a FOV of 32.8" x 32.8". With the 8 mas pixel scale there is a loss of ~3% of the detector area due to vignetting at the corners of the detector as shown in Figure 1.

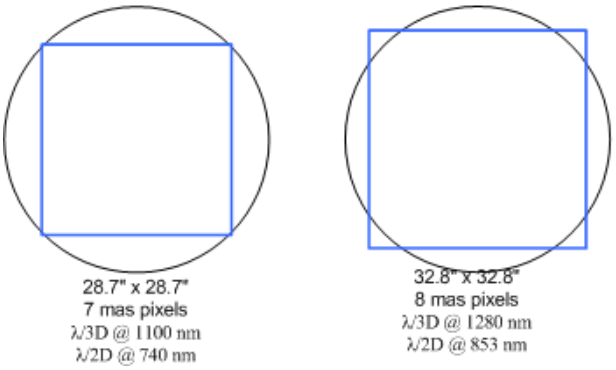

Figure 1: Candidate imager FOVs (blue squares) overlaid on the NGAO science FOV (black circles)

Table 1 lists the cut-on and cut-off wavelengths for the 6 DAVINCI photometric passbands. The sampling obtained in each passband for pixel scales of 7 and 8 mas is illustrated in Figure 2. A more detailed listing of spatial sampling in terms of λ/D for each waveband is provided in the appendix (Table 17).

DAVINCI photometric passband	Wavelength, nm
K band cut-off	2370
K band cut-on	2030
H band cut-off	1780
H band cut-on	1490
J band cut-off	1330
J band cut-on	1170
Y band cut-off	1070
Y band cut-on	970
z band cut-off	922
z band cut-on	818
I band cut-off	853
I band cut-on	700

Table 1: DAVINCI photometric passbands

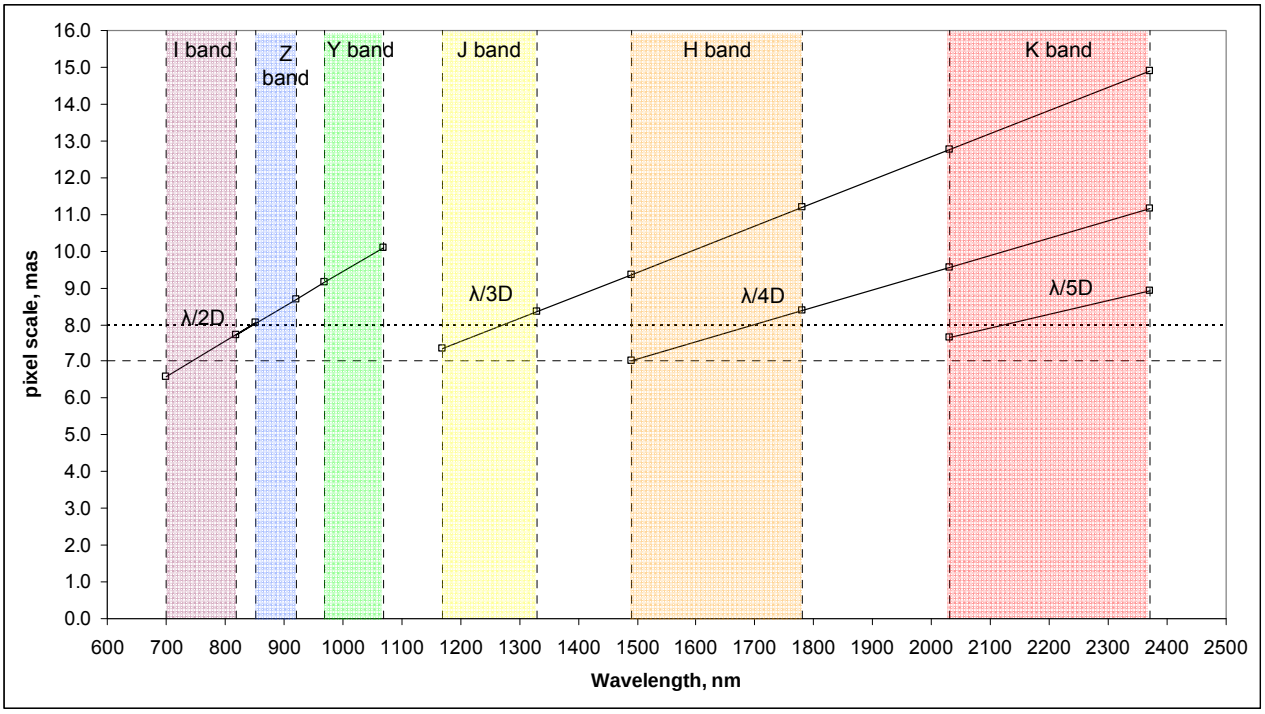

Figure 2: DAVINCI photometric passbands and spatial sampling

From Figure 2 we can see that a 7 mas pixel scale would provide > 2 pixel sampling down to 740 nm in the I band, > 2 pixel sampling in the Z and Y bands, > 3 pixel sampling in the J band, ≥ 4 pixel sampling in H, and > 5 pixel sampling in K band. An 8 mas pixel scale would provide 1 to 2 pixel sampling in I band, > 2 pixel sampling in the Z and Y bands, 2 to 3 pixel sampling in the J band, 3 or more pixel sampling in H, and 4 to 5 pixel sampling in K band. The 8 mas pixel scale would provide the larger FOV.

Limits on Imager Performance due to the AO System

The off-axis performance of the AO system will be limited by anisoplanatic effects, although the central portion of the field will be much more uniformly corrected that the current Keck II AO sytem due to the use of tomographic wavefront reconstruction. An example of the predicted Strehl for field diameters up to 34" is shown in Figure 10 of Dekany et al. (2009).

The NGAO AO relays use off-axis parabolas (OAPs) to collimate the light and to produce a pupil at each deformable mirror (DM). This pupil is located off the optical axis of the OAP collimator, resulting in aberration of the pupil image on the DM (Bauman, 2009). As Bauman shows, for a given field size a smaller DM results in more severe aberrations, the effect of which is to introduce another form of anisoplanatism. This effect will be quantified in a future end to end analysis of the combined performance of the NGAO system including DAVINCI.

The overall pupil image from the AO system exhibits field dependent pupil image shifts and pupil distortions both of which impact the quality of the background suppression obtained from DAVINCI's cold stop. In the current DAVINCI optical design the pupil image at the instrument's cold stop is formed using the first off-axis parabola in an OAP pair that forms the instrument's internal intermediate focal plane. This approach compensates the pupil image and improves cold stop performance.

Spatial distortion of the image at the detector focal plane is an important issue for astrometry. The DAVINCI optical design goal is to keep distortion to < 2% over the full unvignetted area of the detector (Adkins, 2009b). In the current DAVINCI optical design (Adkins et al., 2010) the distortion present is simple barrel distortion with a maximum of 1% over the entire FOV. This level of distortion should be able to be calibrated out using a precision reference grid or other focal plane spatial calibrator.

Detector Pixel Scale and Sensitivity

As noted earlier, adopting a single detector pixel scale dictated by the finest pixel scale needed to properly sample the diffraction limit at the shortest wavelength of interest will result in oversampling at longer wavelengths. This can be expected to have an impact on sensitivity since having more pixels across the FWHM will increase the dark current noise and read noise in the image. At the same time, smaller pixels will see less sky and system background, increasing the permissible exposure time without approaching detector saturation. In the discussion of sensitivities found in the next section of this document we include consideration of the impact of a fixed detector plate scale on performance at longer wavelengths.

IMAGER SENSITIVITY

To predict the sensitivity of the NGAO science imager we need to determine quantities for the total signal and the noise in that signal. The total signal, *S*, in electrons, is described by equation 1. Note that for all calculations we assume a gain of 1 DN per electron.

$$S = (P_{object} \times QE \times N \times t \times Strehl) + (P_{background} \times QE \times N \times t \times Pixels) + (D \times N \times t \times Pixels)$$

where :

P_{object} = object photons/s reaching the detector

QE = the detector manufactur er' s specified detective quantum efficiency ,

i.e. a QE of 1 means each interactin g photon generates 1 electron of signal

N = number of exposures

t = exposure time in seconds

$Strehl$ = Strehl provided by the AO correction

P_{sky} = sky photons/s/ pixel reaching the detector

$P_{background}$ = total background photons/s/ pixel (Sky + telescope +AO) reaching the detector

D = dark current signal in electrons/ pixel/s

$Pixels$ = the number of image pixels

(1)

The predicted average Strehl in each of the AO system passbands based on 170 nm residual wavefront error is computed as the average at the cut-on and cut-off wavelength using the extended Marechal approximation as shown in equation 2 (Hardy, 1998, p. 115).

$$Strehl = e^{-(\sigma_p)^2}$$

where :

$$\sigma_p = 2 \times \pi \times \frac{wfe}{\lambda}$$

and :

wfe = rms wavefront error in nm

λ = wavelength in nm

(2)

The resulting Strehl in each passband is given in Table 2.

Passband	Ave. Strehl (170 nm wavefront error)
I band photometric	15%
Z band photometric	22%
Y band photometric	33%
J band photometric	47%
H band photometric	65%
K' band photometric	77%
K band photometric	79%

Table 2: Predicted Strehl in each photometric passband

If we assume perfect background subtraction then the total object signal S_{object} in electrons is described by equation 3.

$$S_{object} = P_{object} \times QE \times N \times t \times Strehl \tag{3}$$

The required aperture for a diffraction limited image is assumed to be that needed for a well compensated image (Hardy, 1998, p. 42), i.e. a diameter equal to $\frac{2 \times \lambda}{D}$ where D is the diameter of the telescope aperture, and λ is the cut-on (shortest) wavelength in the passband of interest. Based on this assumption we determine the total number of pixels for a point source as shown in equation 4.

$$Pixels = \frac{\pi * \left(206265 * \frac{\lambda}{D} \right)^2}{\theta_{\text{pixel}}{}^2}$$

where :

λ = wavelength in nm $\times 10^{-9}$

D = diameter of telescope aperture in m

θ_{pixel} = angular size of each pixel on the sky in arcseconds (4)

The noise in the signal is described by equation 5.

$$Noise = \sqrt{S_{object} + (P_{background} \times QE \times N \times t \times Pixels) + (D \times N \times t \times Pixels) + (R^2 \times N \times Pixels)}$$

where : (5)

R = rms read noise in electrons per pixel per read

The SNR is then given by equation 6.

$$SNR = \frac{S_{object}}{Noise} \times \sqrt{N} \tag{6}$$

To determine the object photons we use flux densities for Vega as given in Tokunaga and Vacca (2005), Table 1, and estimates for the NGAO I, Z, and Y bands as discussed in appendix A of Adkins and McGrath (2010).

The object flux P_{object} for a given magnitude star (M) in a given passband in units of photons/s is calculated using equation 7.

$$P_{object} = 10^{(-0.4*M)} \times F_\nu \times P_F \times \frac{\Delta\lambda}{\lambda} \times A_{tel} \times T_{atm} \times T_{tel} \times T_{AO} \times T_{filter} \times T_{inst}$$

where:

M = magnitude in a given passband

F_ν = flux in Janskys (from Tokunaga, 2005)

P_F = conversion from Janskys to photons/s/m^2 where 1 Jansky = 1.51×10^7 photons/s/m^2

$\frac{\Delta\lambda}{\lambda}$ = bandpass filter FWHM divided by the central wavelength of the filter (7)

A_{tel} = collecting area of the telescope in m

T_{atm} = transmission of the atmosphere at zenith

T_{tel} = transmission of the telescope

T_{AO} = transmission of the AO system

T_{filter} = passband transmission of the selected filter

T_{inst} = transmission of the instrument

For the calculations presented here we assume an average value for atmospheric transmission, telescope transmission, and AO system transmission over each passband as shown in Tables 2 and 3 of Adkins and McGrath (2010) as well as the DAVINCI imager's zero point magnitudes m_z and the background in magnitudes per square arcsecond for each photometric passband, also in Adkins and McGrath.

IMAGER PERFORMANCE PREDICTIONS

The imager performance predictions are based on the minimum acceptable values for a Hawaii-4RG (H4RG) IR FPA with a 2.5 μm cut-off as described in Adkins (2009a). The relevant parameters for this analysis are summarized in Table 3.

Parameter	Goal Value	Notes
Dark Current	0.01 e^-/s	Median dark current of all imaging pixels
Charge Storage Capacity	100,000 e^-/pixel	Array average number of electrons where the photon transfer curve first deviates from a straight line
Read Noise	15 e^-/pixel	Per CDS read
Quantum Efficiency	0.80 0.75 0.70	970 to 2400 nm 850 to 970 nm 700 to 850 nm

Table 3: Hawaii-4RG performance parameters

Effect of Pixel Scale on Performance

Equation 3 describes the number of pixels assuming a circular aperture for a given pixel scale. The corresponding area is constant for all pixel scales in a given passband and therefore the background contribution is constant for all pixel scales in that passband. The read noise clearly increases as the pixel

scale becomes smaller due to the greater number of pixels that will be read out. The total dark current also increases as the number of pixels increases. Since the K band represents the largest diffraction limited image size, and also has the highest background levels due to thermal sources, we start the analysis of pixel scale using the K band.

The number of pixels in the circular aperture for pixel scales from 100 mas to 5 mas, along with the resulting total read noise contribution, assuming single CDS read noise of 15 e^-/pixel/read, and read noise of 4 e^-/pixel/read for 16 Fowler samples (performance recently demonstrated by H2RG detector testing in the MOSFIRE project, Kulas, 2010) is shown for the K band aperture size (0.076" diameter) in Table 4.

Pixel scale, mas	**100**	**50**	**20**	**15**	**10**	**8**	**7**	**5**
Number of pixels, K band	1.0	1.8	11.5	20.4	46.0	71.8	93.8	183.8
Total read noise, e^-, single CDS	15.0	20.3	50.8	67.8	101.7	127.1	145.3	203.4
Total read noise, e^-, 16 Fowler samples	4.0	5.4	13.6	18.1	27.1	33.9	38.7	54.2

Table 4: Number of pixels and total read noise for the K band aperture size at various pixel scales

As expected, a smaller pixel scale results in increased read noise. It should be noted that in the following performance analysis for point sources we ignore the fact that we actually have a square aperture with an integer number of pixels.

Point Source Sensitivity

Assuming perfect background subtraction, the point source magnitude required to reach an SNR of 5 in one hour (four 900 s exposures) for the K band are shown in Table 5 and Figure 3.

Pixel scale, mas	**100**	**50**	**20**	**15**	**10**	**8**	**7**	**5**
K band magnitude	25.58	26.00	26.00	26.00	26.00	26.00	26.00	26.00

Table 5: K band magnitudes for an SNR of 5 in one hour

Note that the assumption that the collection aperture cannot be less than 1 pixel in diameter penalizes the 100 mas pixel scale by increasing the area from the diffraction limited value of 3.6 mas^2 to 10 mas^2, resulting in an increase in the sky background. There is essentially no difference in the sensitivity for pixel scales from 50 to 5 mas.

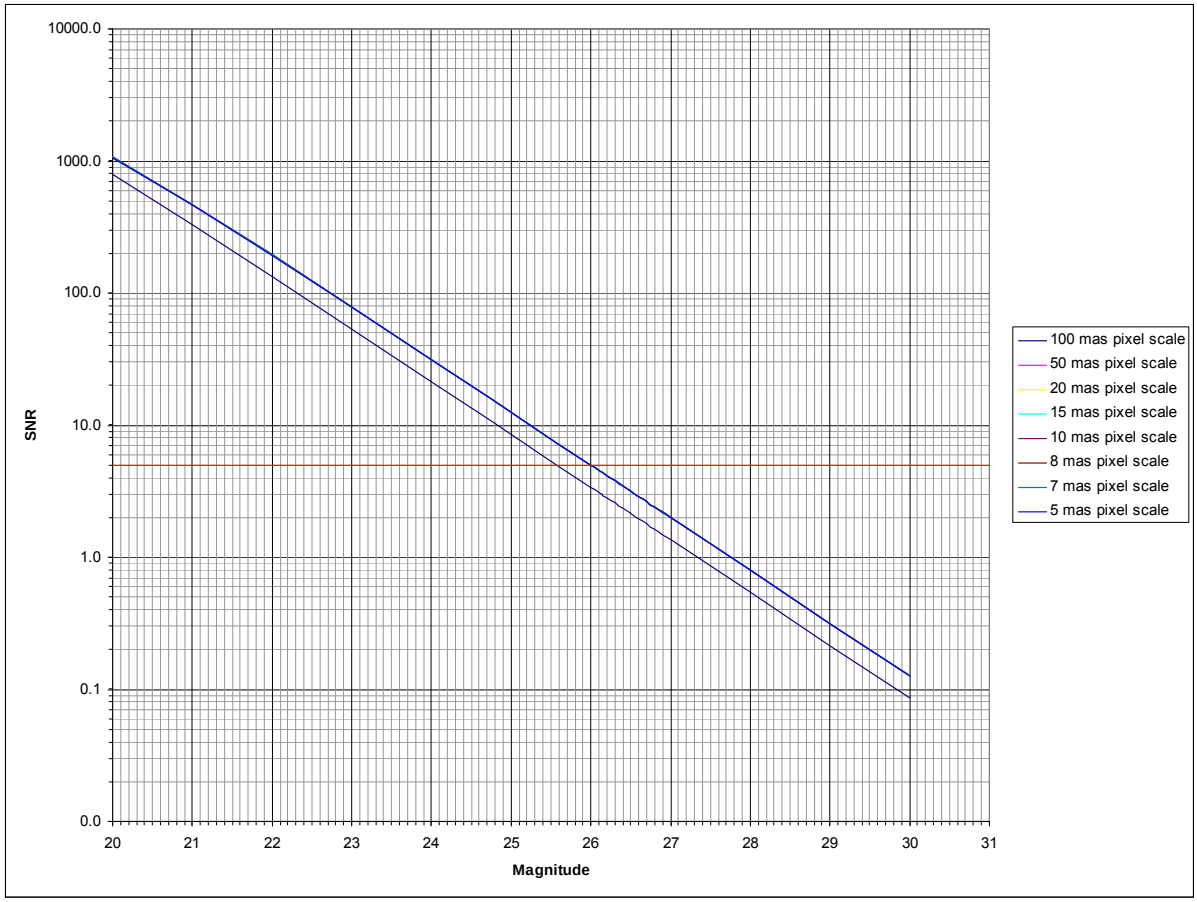

Figure 3: K band magnitudes vs. pixel scale for a 1 hour exposure
An SNR of 5 is indicated by the red line.

Background Limited Exposure Times

The SNR as a function of magnitude, for both a background limited exposure, and an exposure including read noise was calculated for the 7, 8, and 10 mas pixel scales using exposure times from 10 to 1000 s. The result for the 7 mas pixel scale is shown in Figure 4. In the Figure the solid lines are the resulting SNR at each exposure time including read noise, and the dashed lines are the SNR for a background limited exposure. Where the lines are co-incident for a given exposure time the exposure has become background limited. This is achieved at ~120 s with an SNR difference between the exposure with read noise and a background limited exposure of 0.9% for K = 27. For the same exposure time and magnitude the 8 mas pixel scale is about 0.2% better, and the 10 mas pixel scale is about 0.5% better.

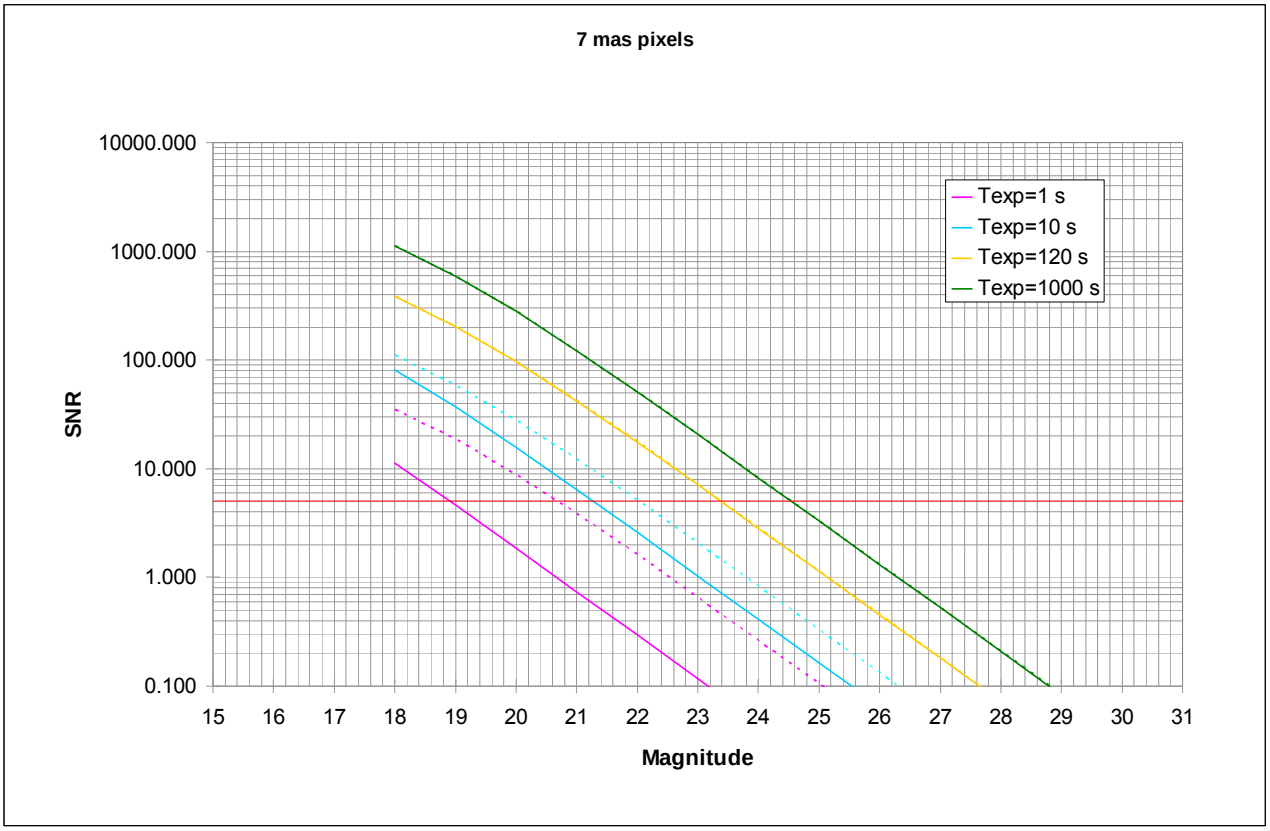

Figure 4: SNR vs. K band magnitude for 1, 10, 100, 120, and 1000 s exposures and a 7 mas pixel scale
An SNR of 5 is indicated by the red line. The dashed lines are for background limited conditions.

Maximum Exposure Time

Another consideration with respect to pixel scale is the maximum duration for a single exposure before a pixel is saturated. Smaller pixels allow a longer exposure for a given flux level, assuming a constant area on the sky. For the expected K band sky background magnitude of 13.42 per square arc second (Adkins & McGrath, 2010) the maximum time for a single exposure in K band to 50% of the detector's full charge storage capacity at each of the pixel scales in Table 4 is shown in Figure 5.

The maximum exposure time to 50% of the typical value for the H4RG detector's maximum charge storage capacity of 100,000 e^- is ~34 s for the 100 mas scale, and increases to ~3700 s for the 8 mas scale, and ~4420 s for the 7 mas scale. This estimate includes the effect of detector dark current, but with rate of 0.01 e^-/s the effect on the maximum exposure time is small.

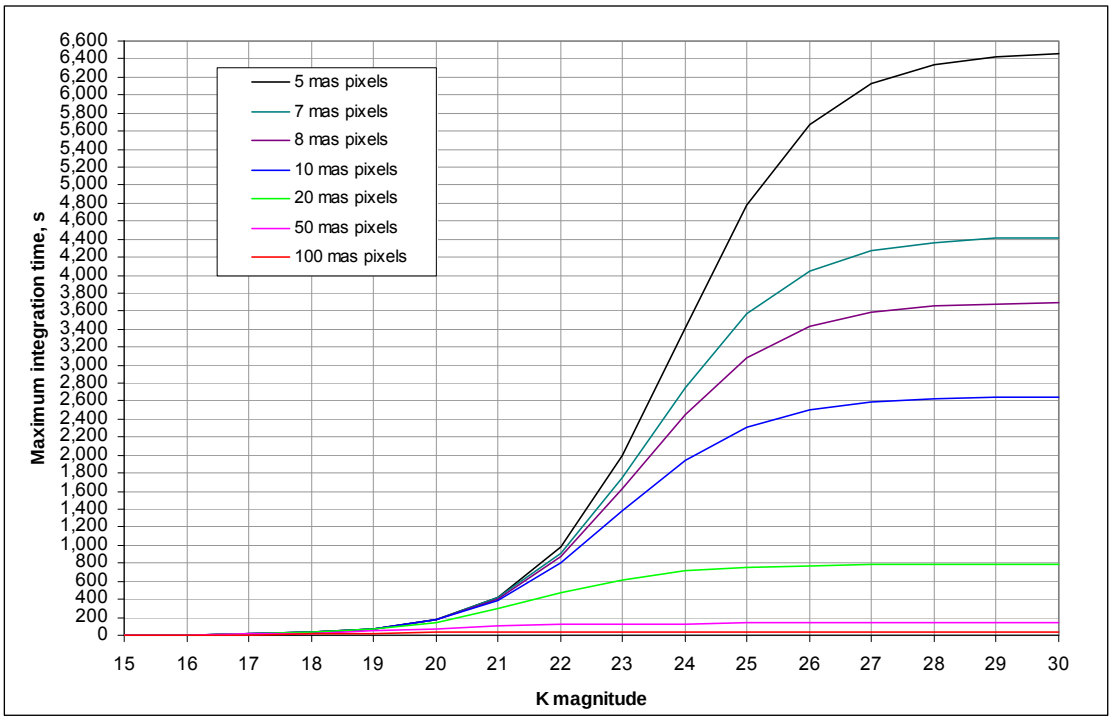

Figure 5: Maximum exposure time (to 50% of full charge storage capacity) vs. K magnitude

Performance Predictions for all Wavelengths

The magnitudes to reach an SNR of 5 in each of the DAVINCI imaging passbands as a function of pixel scale are given in Table 6 and shown graphically in Figure 6. The I and Z band values are based on four 120 s exposures, the Y through K band values are based on four 900 s exposures.

Pixel scale, mas	100	50	20	15	10	8	7	5
I band magnitude	26.10	26.84	27.54	27.47	27.32	27.18	27.10	26.84
Z band magnitude	26.00	26.75	27.33	27.28	27.18	27.10	27.05	26.85
Y band magnitude	26.85	27.60	28.05	28.05	28.05	28.05	28.05	28.03
J band magnitude	26.62	27.38	27.65	27.65	27.65	27.65	27.65	27.63
H band magnitude	25.84	26.60	26.60	26.60	26.60	26.60	26.60	26.60
K' band magnitude	25.80	26.25	26.25	26.25	26.25	26.25	26.25	26.25
K band magnitude	25.58	26	26	26	26	26	26	26

Table 6: Point source magnitudes for an SNR of 5

Figure 6 illustrates the fact that once the exposure time exceeds the background limited exposure time (Table 7), sampling scales between 7 and 50 mas have no impact on sensitivity in the J, H, and K bands. For the Y band a sampling scale between 7 and 20 mas has no impact on sensitivity. The curves for the I and Z bands illustrate the fact that the total exposure time of 480 s used here is not background limited. By increasing the exposures in Z band to 1200 s per frame for a total of 4800 s uniform

sensitivity is obtained from 7 to 20 mas, with similar results in I band using 6 exposures of 1200 s for a total exposure time of 7200 s.

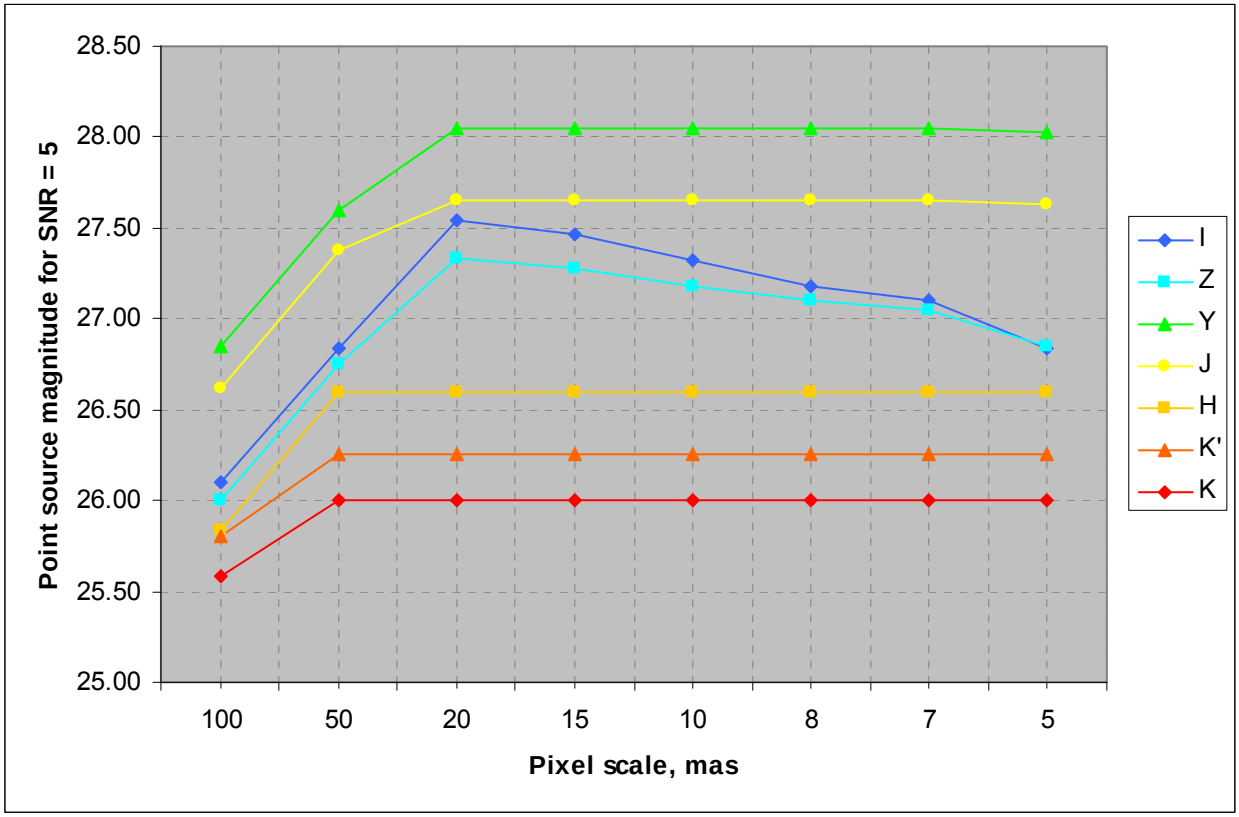

Figure 6: Point source magnitudes for an SNR of 5

The background limited exposure time for each of the imaging passbands with a point source magnitude of 27 are given in Table 7 for the 10, 8, and 7 mas pixel scales.

Pixel scale, mas	10	8	7
I band	1.2 h	1.7 h	2.2 h
Z band	0.7 h	1.1 h	1.3 h
Y band	1200 s	1800 s	2400 s
J band	360 s	560 s	720 s
H band	45 s	70 s	100 s
K' band	81 s	126 s	180 s
K band	60 s	90 s	120 s

Table 7: Background limited exposure time in s

The maximum exposure times to 50% of the typical value for the H4RG detector's maximum charge storage capacity of 100,000 e^- are given in Table 8 for the 10, 8, and 7 mas pixel scales in each of the imaging passbands assuming a point source magnitude of 30.

Pixel scale, mas	10	8	7
I band	11953	12120	12191
Z band	11540	11842	11972
Y band	10538	11143	11416
J band	7858	9048	9657
H band	2184	3104	3765
K' band	3494	4712	5512
K band	2647	3692	4419

Table 8: Maximum exposure time in s to 50% of detector charge storage capacity

Conclusions

For the infrared bands the sky background is the dominant factor in the SNR as indicated by the relatively short exposure times required to reach a background limited exposure. This is also reflected in the limited impact on 5σ magnitude for the range of pixel scales from 20 mas to 5 mas as shown in Figure 6. This suggests there is no compelling sensitivity argument to guide the selection of pixel scale in the range of choices that address the diffraction limited sampling requirements for DAVINCI, and also indicates that oversampling at longer wavelengths does not result in a penalty on SNR.

On the other hand, within the infrared bands the sky background does limit the maximum exposure time before either the accumulated charge rises to the point where the detector's response becomes non-linear or saturates. Here, smaller pixels are better, allowing significantly longer exposure times.

Finally, when the benefit of a larger field of view is considered it seems logical to consider either the 7 or 8 mas pixel scale as the best choice. When sampling vs. wavelength is considered it is desirable to choose the smaller scale since this will provide 2 pixel sampling over most of the I band. As a result we have selected the 7 mas pixel scale for the DAVINCI imager, providing a 28.7" x 28.7" FOV with a H4RG detector.

COMPARISON TO NIRC2

A comparison of the sensitivity of DAVINCI to NIRC2 has been made using the same methodology for NIRC2 as we have used for the sensitivity estimates for DAVINCI. This comparison required research across several of the NIRC2 instrument web pages, the NIRC2 manual, and the NIRC2 SNR and efficiency calculator (WMKO, n. d.). In this process some inconsistencies were noted. One of the most important is the difference between the zero points used in the calculator (found by examination of the calculator source code) and the zero points listed on the sensitivity web page (WMKO, 2004). Using the sensitivities on the sensitivity web page require what seem to be unrealistically low AO system and instrument transmissions to even begin to approach the K band background value for NIRC2 reported on the NIRC2 filters web page (WMKO, 2003). Changing the background spreadsheet (Adkins & McGrath, 2010) to reduce the AO system transmission by 50% from the value obtained from Bouchez (2007), and reducing the assumed NIRC2 transmission to 37% results in K band background of 13.52, much lower than what is reported for the measured background value. As a result we have used the NIRC2 zero points obtained from examining the source code of the NIRC2 SNR and

efficiency calculator. The zero points for the DAVINCI imager and NIRC2 are summarized in Table 9 for the J, H, and K bands. These are similar enough that for background limited exposures on the same AO system one might expect similar performance from both instruments in terms of sensitivity.

Band	Zero point	
	DAVINCI	NIRC2
J	26.96	26.90
H	26.95	26.96
K	26.35	26.18

Table 9: DAVINCI and NIRC2 zero points

We validated the DAVINCI sensitivity estimates for NIRC2 using the NIRC2 SNR and efficiency calculator. A screen shot of this calculator is shown in Figure 7. Examination of the code for the NIRC2 exposure calculator reveals that the "coadds" value is only used to calculate the total exposure time, it is not used to increase the SNR by $\sqrt{N}$ (where N = number of exposures). The values shown in Figure 7 correspond to the conditions used in the K band sensitivity estimates for NIRC2 assuming a 10 mas pixel scale (the NIRC2 narrow camera pixel scale) and a K band Strehl of 31% for the Keck II AO system with a measured 378 nm total wavefront error in LGS mode with a 10th magnitude NGS (Wizinowich et al., 2007, p. 2).

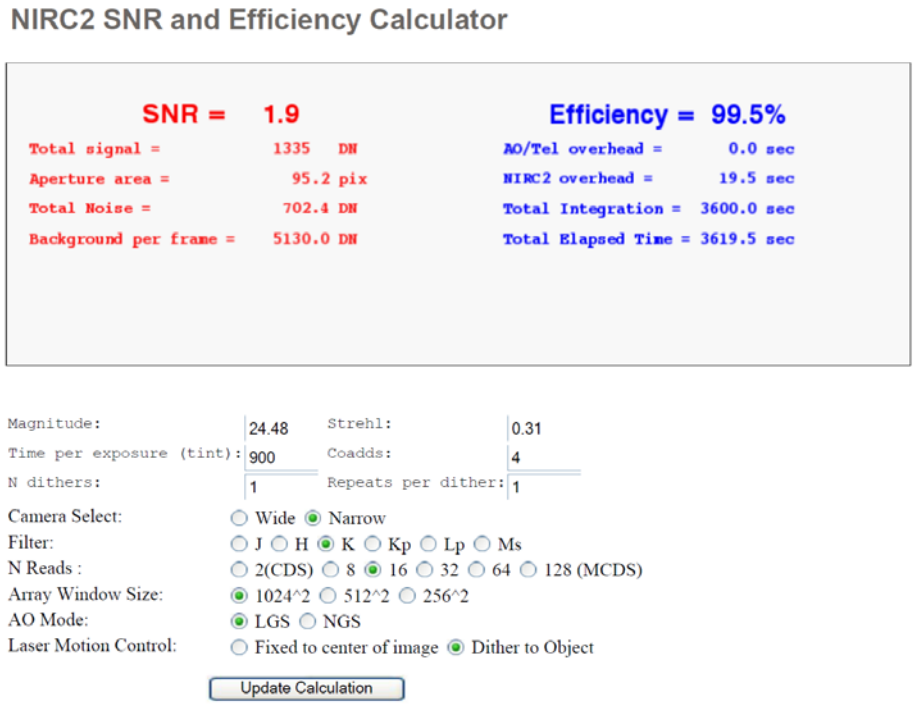

Figure 7: NIRC2 SNR and efficiency calculator screen shot

The DAVINCI sensitivity estimate for NIRC2 under the same conditions gives an SNR of 5. Without including the effect of using 4 exposures to reach the 3600 s total exposure time the SNR from the DAVINCI sensitivity estimate is 2.5. Part of the remaining difference comes from the assumed value

for the NIRC2 K band background used in the calculator. The calculator uses background count rate of 22.8 e-/s/pixel which does not match the measured NIRC2 background (it is low by ~4 e-/s/pixel), and uses a larger aperture (95.2 pixels) than the DAVINICI estimate which assumes an aperture of 46 pixels. When these changes are made the DAVINCI estimate matches the NIRC2 calculator SNR.

As discussed in Adkins and McGrath (2010) the background estimates for DAVINCI were validated by comparison to the measured values on WMKO NIRC2 filters web page. We found that by adjusting the temperature for the Keck II AO system we could match the K band measured background and obtain reasonable agreement for the H band. We could not obtain agreement for the J band. The measured J band background is ~1.2 magnitudes brighter than our estimate. In comparing the sensitivity of NIRC2 and DAVINCI we have used the estimated values for NIRC2 rather than penalize NIRC2 in J band by using the higher measured background.

The detector in NIRC2 (a 1024 x 1024 pixel InSb Aladdin-3 array with 27 μm pixels) has a much smaller full well (18,000 e^- to 5% non-linearity) than the H4RG (100,000 e^- minimum with < 1% non-linearity). Because of the increased non-linearity when approaching full well, and the recommendation is to limit the exposure to ~32% of full well (~5, 700 e^-) based on the maximum K band exposure time of 630 s listed on the NIRC2 sensitivity web page. When the higher background count rate from background estimate discussed above and the zero point magnitude from the exposure time calculator is used, the DAVINCI calculations applied to NIRC2 gives a maximum exposure time in K band of 140 s (including read noise and dark current).

When the values used on the NIRC2 sensitivities spreadsheet of 12.24 for the K band background, and 24.63 for the zero point are used, the result is 637 s, if read noise and dark current are omitted, and 249 s with read noise and dark current included. For the analysis presented here we have used 128 s as the maximum exposure time, and assumed 16 Fowler reads per exposure. 28 exposures of 128 s results in a total exposure time of 3,584 s. We assume that there are 7 coadds, resulting in 4 frames being read out, and we assume that the SNR is improved by the square root of the number of frames read out. We assume that coadds do not improve the SNR.

The results comparing the DAVINCI imager with a pixel scale of 7 mas, to the NIRC2 narrow camera (10 mas pixel scale) in the J, H, and K bands are shown in Table 10.

Band	Strehl		Point source magnitude (SNR = 5)		Background limited exposure time, s		Background (mag./square arc second)	
	DAVINCI	NIRC2	DAVINCI	NIRC2	DAVINCI	NIRC2	DAVINCI	NIRC2
J	47%	3%	27.65	24.6	720	4800	16.04	16.07
H	65%	12%	26.60	24.76	100	540	13.76	13.76
K	79%	31%	26.00	24.48	120	380	13.42	12.6

Table 10: DAVINCI imager compared to NIRC2 narrow camera

IFS PERFORMANCE PREDICTIONS

Accurately comparing the DAVINCI IFS to OSIRIS is much more difficult than comparing the DAVINCI imager to NIRC2 for several reasons. The most significant reason is the complexity of what happens beyond the lenslet plane in the spectrograph optics. As discussed in the OSIRIS user's manual (Larkin et al., 2010, p. 22, p. 62) the spectrum from each lenslet is spread over more than 1 pixel, and for each spectrum there are systematic effects in the optics that result in different efficiencies over the integral field. Zero points for the OSIRIS spectrograph have only been calculated for the spectrograph for broadband mode, and the available data for measured backgrounds is very limited.

The approach taken here is to compute the backgrounds, zero points, and sensitivity on a per lenslet basis. The same approach used to estimate backgrounds for NIRC2 (Adkins & McGrath, 2010) is used to compute the backgrounds and zero points for OSIRIS and DAVINCI. For OSIRIS the filter characteristics for each passband are taken from Table 2-2 of Larkin et al. (2010, p. 15). The instrument's transmission in each passband are taken from Table 2-6 of Larkin et al. (p. 21) using the measured filter transmission for each passband from Table 2-2, and using the October 2009 measurement of the grating efficiency at 1.308 μm in the 5th order for the J band grating efficiency (Larkin, private communication, 2010). The resulting transmission assumptions for OSIRIS broadband filters and for OSIRIS narrowband filters that are closest to corresponding DAVINCI IFS narrowband filters in the J, H, and K bands are shown in Table 11 and Table 12. The values used for the collimator and camera three mirror anastigmats (TMAs) assume some coating degradation due to dirt from various environmental exposures during instrument servicing.

	J band	H band	K band
Window	97%	97%	97%
Fold Mirrors	96%	96%	96%
Collimator Lens	96%	96%	96%
Filters	79%	93%	86%
Camera Lens	96%	96%	96%
Lenslet Array (AR Coated, 2 surfaces)	95%	95%	95%
TMA Collimator (4 mirrors, includes first fold)	92%	92%	92%
Grating (varies with wavelength)	30%	42%	42%
Camera Optics (4 mirrors, includes fold)	92%	92%	92%
Total Optical Throughput	**16%**	**27%**	**25%**

Table 11: OSIRIS throughput for broadband filters in J, H, and K bands

	Jn2	Hn4	Kn4
Window	97%	97%	97%
Fold Mirrors	96%	96%	96%
Collimator Lens	96%	96%	96%
Filters	78%	83%	75%
Camera Lens	96%	96%	96%
Lenslet Array (AR Coated, 2 surfaces)	95%	95%	95%
TMA Collimator (4 mirrors, 99%; includes first fold)	92%	92%	92%
Grating (varies with wavelength)	30%	42%	42%
Camera Optics (4 mirrors, 99%; includes fold)	92%	92%	92%
Total Optical Throughput	**16%**	**24%**	**22%**

Table 12: OSIRIS throughput for selected narrowband filters in J, H, and K bands

Values for the detector quantum efficiency are needed to calculate zero points; these values are taken from Figure A-7 (Larkin et al., 2010, p. 77) for 70 K detector operating temperature, using 0.55 for J band, 0.65 for H band, and 0.8 for K band. The zero points given in the Table 2-7 of Larkin et al. (p. 22) for broad band in J, H, and K are shown in Table 13 along with the calculated zero points, the measured NIRC2 backgrounds (Adkins & McGrath, 2010), the OSIRIS measured backgrounds (where available) and the calculated backgrounds.

	Zero points		**Backgrounds (mag./sq. arcsecond)**		
	OSIRIS Table 2-7	**OSIRIS calculated value**	**NIRC2 measured value**	**OSIRIS measured value**	**OSIRIS calculated value**
J band	23.5	25.48	14.9	-	14.1
H band	24.3	25.85	13.6	-	12.2
K band	23.7	25.34	12.6	11.8	11.0

Table 13: OSIRIS broadband zero points and backgrounds

Note that the calculated zero points are much higher than the values provided in the OSIRIS manual. We understand that these were estimated from broadband spectra, but for consistency we are using the same method as we have used to estimate the sensitivity for DAVINCI in order to make the comparison fairer since we don't have complete documentation on the method used for the zero points given in the OSIRIS manual.

The corresponding narrowband zero points and backgrounds for OSIRIS and DAVINCI are shown in Table 14.

Band DAVINCI/OSIRIS	**Zero points**		**Background (mag./square arc second)**	
	DAVINCI	**OSIRIS**	**DAVINCI**	**OSIRIS**
Jb/Jn2	25.62	23.95	15.83	15.50
Hc/Hn4	24.76	24.22	13.76	13.92
Kc/Kn4	24.16	23.73	13.72	12.27

Table 14: DAVINCI and OSIRIS narrowband zero points and background comparison

To calculate the sensitivity per lenslet we use the following equation (8) for OSIRIS:

$$SNR_{lenslet} = \frac{S_{lenslet} \times N \times t}{\sqrt{(S_{lenslet} \times N \times t) + (Background_{lenslet} \times N \times t) + (D \times N \times t \times channels) + (R^2 \times N \times channels)}} \times \sqrt{N}$$

where :

$S_{lenslet}$ = object signal in electrons/s in each lenslet computed from the zero point

N = number of exposures

t = exposure time in seconds (8)

$Background_{lenslet}$ = total background electrons/s/lenslet (Sky + telescope +AO)

D = dark current signal in electrons/pixel/s

$channels$ = the number of spectral channels per lenslet

R = rms read noise per channel in electrons/read

We accept a small inaccuracy in the form of this equation by using the number of spectral channels, rather than the number of pixels per lenslet to calculate the read noise and dark current noise. The estimate for read noise per spectral channel given in the OSIRIS manual (Larkin et al., 2010, p. 22) of 10 e- for extracted spectra is used here, and we allow the dark current to be under estimated by using the number of channels instead of the corresponding number of pixels. We assume 428 spectral channels per lenslet (the average number of channels for the selected narrowband filters).

For DAVINCI we use the same approach, but here we use the actual number of pixels per lenslet (1360) instead of the number of spectral channels (680) to compute the read noise and dark current noise.

The resulting magnitudes in each band to reach an SNR of 5 with 4 exposures of 900 s each and a 35 mas sampling scale is shown for DAVINCI and OSIRIS in Table 15.

Band DAVINCI/OSIRIS	Strehl		Point source magnitude (SNR = 5)		Background (mag./square arc second)	
	DAVINCI	OSIRIS	DAVINCI	OSIRIS	DAVINCI	OSIRIS
Jb/Jn2	47%	3%	26.1	20.97	15.83	15.50
Hc/Hn4	65%	12%	24.8	22	13.76	13.92
Kc/Kn4	79%	31%	23.9	21.75	13.72	12.27

Table 15: DAVINCI and OSIRIS sensitivity and background comparison

Re-calling that the background computed for the narrowband filter in K is higher than what is indicated in the OSIRIS manual, that is 11 vs. 11.8, we also computed the background per lenslet for the 50 mas scale using the OSIRIS Kn4 filter and compared it with data supplied by Jim Lyke (private communication, 2010). The computed background is 96 e^-/s/lenslet, while a dark subtracted background taken from a representative sky image from OSIRIS over 1024 x 1204 pixel box at the center of the detector gives 0.183 e^-/s/pixel or 157 e^-/s/lenslet, assuming 2 pixels per spectral channel and 428 spectral channels. This suggests we are not unduly penalizing OSIRIS with excess

background, and that the broad band figure of K = 11.8 mag./sq. arc second for the 35 and 50 mas pixel scales (Larkin et al., 2010, p. 10) may be low.

Finally, the reader may be aware that improvements have been proposed for OSIRIS, in particular the possibility that a new grating may be possible with efficiencies approaching 60% in all three bands discussed here. While this is still a somewhat speculative possibility pending further study later in 2010, we show in Table 16 the effect of improving the grating efficiency assumed in Table 12 to 60% for all three narrow bands.

Band DAVINCI/OSIRIS	Strehl		Point source magnitude (SNR = 5)		Background (mag./square arc second)	
	DAVINCI	OSIRIS	DAVINCI	OSIRIS	DAVINCI	OSIRIS
Jb/Jn2	47%	3%	26.1	21.65	15.83	14.74
Hc/Hn4	65%	12%	24.8	22.3	13.76	13.55
Kc/Kn4	79%	31%	23.9	21.91	13.72	11.9

Table 16: DAVINCI and OSIRIS sensitivity and background comparison, new OSIRIS grating

Note that the improvement in grating efficiency from 42% to 60% in H and K improves the corresponding zero points to 24.59 and 24.1 respectively. The improvement in grating efficiency from 30% to 60% in J improves the corresponding zero point to 24.7.

The resulting modest improvement in sensitivity is attributed to the fact that when we improve the throughput (by 2x in J) we also increase the background magnitude. We can also consider improvements due to replacement of the detector, changing from a Hawaii-2 to a Hawaii-2RG. This can be expected to improve the QE in J and H band relative the values assumed here (by ~ 25% in J and 15% in H band), to reduce the dark current by about 3 times, and slightly reduce the read noise (from ~ 5 e-/pixel/read to ~ 4 e-/pixel/read for up the ramp or Fowler sampling with 16 samples). However, the impact of this change is difficult to quantify because of the additional noise due to the overlapping spectral PSFs at the detector and because of the complexities of data reduction in OSIRIS. We have elected not to attempt any representative calculations for an improved detector in OSIRIS at this time, and a more sophisticated modeling approach for both DAVINCI and OSIRIS will need to be used to refine the estimates given here.

REFERENCES

Adkins, S. (2009, January 20). Keck Next Generation Adaptive Optics Detectors for NGAO Instrumentation. Keck Adaptive Optics Note 556. Waimea, HI: W. M. Keck Observatory.

Adkins, S. (2009, September 14). NGAO science instrumentation: Design Concept. Waimea, HI: W. M. Keck Observatory.

Adkins, S., & McGrath, E. (2010, May 11). DAVINCI background and zero point estimates (KAON 764). Waimea, HI: W. M. Keck Observatory.

Adkins, S., Kupke, R., Panteleev, S., Pollard, M., & Thomas, S. (2010, June). Preliminary Design Report for DAVINCI: the Diffraction limited Adaptive optics Visible and Infrared iNtegral field spectrograph and Coronagraphic Imager (KAON 761). Waimea, HI: W. M. Keck Observatory.

Adkins, S., Larkin, J., Max, C. & McGrath, E. (2009, July 3). NGAO science instrumentation baseline capabilities summary. Waimea, HI: W. M. Keck Observatory.

Baek, M. & Marchis, F. (2007, November 27). Next Generation Adaptive Optics: Optimum pixel sampling for asteroid companion studies. Keck Adaptive Optics Note 529. Waimea, HI: W. M. Keck Observatory.

Bauman, B. J. (2009). Anisoplanatism in adaptive optics systems due to pupil aberrations.

Bouchez, A. (2007, August 28). Keck Next Generation Adaptive Optics background and transmission budgets, version 1.1. Keck Adaptive Optics Note 501. Pasadena, CA: Caltech Optical Observatories.

Dekany, R., Neyman, C., Wizinowich, P., McGrath, E. & Max, C. (2009, March 10). Build-to-cost architecture wavefront error performance. Keck Adaptive Optics Note 644. Waimea, HI: W. M. Keck Observatory.

Hardy, J. W. (1998). *Adaptive optics for astronomical telescopes*. Oxford, UK: Oxford University Press.

Kulas, K. (2010, January). MOSFIRE detector testing status. Retrieved January 15, 2010 from http://irlab.astro.ucla.edu/mosfire/team/meetings/meeting63/20100115-MOSFIRE%20Detector-Kulas.ppt

Kupke, R. (2009, October 27). NGAO optical relay design. Keck Adaptive Optics Note 685. Santa Cruz, CA: UCO/Lick Observatory.

Larkin, J., Barczys, M., McElwain, M., Perrin, M., Jason Weiss, J., & Wright, S. (2010, March 1). OSIRIS: OH-Suppressing Infra-Red Imaging Spectrograph, users' manual. Version 2.3. Los Angeles, CA: UCLA Infrared Laboratory.

Smith, W. J. (2000). *Modern Optical Engineering*. New York, NY: McGraw-Hill.

Tokunaga, A. T. & Vacca, W. (2005, April). The Mauna Kea Observatories near-infrared filter set. III. Isophotal wavelengths and absolute calibration. *The Publications of the Astronomical Society of the Pacific, 117*(830), 421-426. Chicago, IL: University of Chicago Press.

Wizinowich, P., Dekany, R., & van Dam, M. (2007, March 5). Wavefront Error Budget Predictions and Measured Performance for Current and Upgraded Keck Adaptive Optics. Keck Adaptive Optics Note 461. Waimea, HI: W. M. Keck Observatory.

W. M. Keck Observatory. (2004, April). NIRC2 sensitivity. Retrieved December 9, 2009 from http://www2.keck.hawaii.edu/inst/nirc2/sensitivity.html

W. M. Keck Observatory. (2003, February 29). NIRC2 filters. Retrieved December 9, 2009 from http://www.keck.hawaii.edu/realpublic/inst/nirc2/filters.html

W. M. Keck Observatory. (n. d.). NIRC2 signal to noise and efficiency calculator. Retrieved December 9, 2009 from http://www2.keck.hawaii.edu/cgi-bin/ion-p?page=nirc2_snr_eff.ion

APPENDIX

Passband	Wavelength, nm	λ/D (")	λ/D (mas)	λ/2D (mas)	λ/3D (mas)	λ/4D (mas)	λ/5D (mas)
K band cut-off	2370	0.045	44.7	22.3	14.9	11.2	8.9
K band cut-on	2030	0.038	38.2	19.1	12.7	9.6	7.6
H band cut-off	1780	0.034	33.5	16.8	11.2	8.4	6.7
H band cut-on	1490	0.028	28.1	14.0	9.4	7.0	5.6
J band cut-off	1330	0.025	25.1	12.5	8.4	6.3	5.0
J band cut-on	1170	0.022	22.0	11.0	7.3	5.5	4.4
Y band cut-off	1070	0.020	20.2	10.1	6.7	5.0	4.0
Y band cut-on	970	0.018	18.3	9.1	6.1	4.6	3.7
Z band cut-off	922	0.017	17.4	8.7	5.8	4.3	3.5
Z band cut-on	818	0.015	15.4	7.7	5.1	3.9	3.1
I band cut-off	853	0.016	16.1	8.0	5.4	4.0	3.2
I band cut-on	700	0.013	13.2	6.6	4.4	3.3	2.6

Table 17: Diffraction limited image size and corresponding pixel scale for 2 to 5 pixel sampling for the six NGAO photometric wavelength bands, the cut-off wavelengths are indicated by gray shading